Submission type: Article - Discoveries

Title: Uncovering the genomic basis of infection through co-genomic sequencing of hosts and parasites

Authors: Eric Dexter[1]*, Peter D. Fields[1], and Dieter Ebert[1]

Affiliations:

[1]Department of Environmental Sciences, The University of Basel; Basel, 4051, Switzerland

*Corresponding author email: eric.dexter@unibas.ch

Short title: Co-genomic sequencing of hosts and parasites

Abstract:

Understanding the genomic basis of infectious disease is fundamental objective in coevolutionary theory with relevance to healthcare, agriculture, and epidemiology. Models of host-parasite coevolution often assume that infection requires specific combinations of host and parasite genotypes. Coevolving host and parasite loci are therefor expected to show associations that reflects an underlying infection/resistance allele matrix, yet little evidence for such genome-to-genome interactions has been observed among natural populations. We conducted a study to search for this genomic signature across 258 linked host (*Daphnia magna)* and parasite (*Pasteuria ramosa)* genomes. Our results show a clear signal of genomic association between multiple epistatically-interacting loci in the host genome, and a family of genes encoding for collagen-like protein in the parasite genome. These findings are supported by laboratory-based infection trials, which show strong correspondence between phenotype and genotype at the identified loci. Our study provides clear genomic evidence of antagonistic coevolution among wild populations.

Keywords: Coevolution, parasite, GWAS, daphnia, pasteuria, genome-to-genome, co-genomics

INTRODUCTION

Parasites (including pathogens) infect nearly all forms of life, acting as a fundamental biological force that shapes the evolution of their hosts and drives the dynamics of entire communities (Poulin 2011; Schmid-Hempel 2021). The evolutionary processes among host and parasite are tightly interconnected: As a host population evolves in response to the threat caused by its parasites, so too does the parasite evolve in response to its host. This antagonistic coevolution may be responsible for much of the genetic diversity found in natural populations, promoting local adaptation and population differentiation (Morand 2015; Ebert and Fields 2020). Various models of host-parasite coevolution have been developed to accommodate the fact that phenotypic traits under selection may have different genomic architectures. Under highly specific models of host-parasite interactions, such as the matching-allele and the gene-for-gene models, infections are only possible between specific combinations of host and parasite genotypes (Agrawal and Lively 2002). Parasites will therefore experience high fitness when compatible alleles are common in the host population, and low fitness when such alleles are rare, thus driving a time-lagged cycle of negative-frequency dependent selection which is sometimes known as the Red Queen model of coevolution (Ebert and Fields 2020).

Red Queen evolutionary dynamics are predicted to yield several diagnostic characteristics in both host and parasite genomes. As negative-frequency dependent selection promotes the maintenance of genetic diversity, affected loci are expected to exhibit locally elevated nucleotide diversity relative to other genomic regions (Ebert and Fields 2020). This is because selection is tied to allele frequencies, with common variants being selected against. Highly specific models of host-parasite interactions also predict that certain combinations of host and parasite alleles are unlikely to be found in infected hosts, even if both alleles occur in the population at large. Coevolving host and parasite loci are therefore expected to show a statistical pattern of association that reflects the underlying infection/resistance allele matrix (Ebert and Fields 2020). The non-random association of alleles across the genomes of two interacting species can be considered as a form of interspecies linkage disequilibrium, more succinctly "interlinkage." Interlinkage is a predicted consequence of genomic interactions between hosts and parasites and thus direct evidence for ongoing coevolutionary interactions of the antagonists. Despite arising as a fundamental prediction of host-parasite coevolution, there is little empirical evidence of interlinkage among naturally coevolving populations.

Here we present clear evidence of interlinkage among natural populations of the planktonic crustacean *Daphnia magna* and its endoparasitic bacterium *Pasteuria ramosa* (Firmicutes).

Daphnia magna is a common planktonic microcrustacean that inhabits standing fresh and brackish waters across most of the northern hemisphere. Wild populations of *D. magna* are often heavily parasitized by a wide variety of bacteria, virus, and microsporidian species, including the endospore-forming bacteria *Pasteuria ramosa* (Ebert 2005). *Daphnia magna* ingest planktonic spores of *P. ramosa* during filter feeding, which enter the digestive tract along with food and other particulate matter and may attach to the gut lining. After attachment and penetration of the host cuticle, *P. ramosa* rapidly proliferate in the body cavity of the host (Ebert et al. 1996). During *P. ramosa* infections, the normally transparent host body cavity is completely filled with opaque spores which will be released into the environment upon death of the host. *P. ramosa* infection spreads exclusively through horizontal transmission from host to host.

The *D. magna* / *P. ramosa* infection process appears to be governed by highly specific interactions, such that *D. magna* genotypes (aka. clones) are either completely susceptible or completely resistant to particular strains of *P. ramosa* (Bento et al. 2017; Bento et al. 2020). This binary outcome is strongly linked to the attachment of the parasite to the host cuticle. This highly-specific attachment step is hypothesized to be governed by interactions between *P. ramosa* surface proteins and highly-polymorphic extracellular proteins at the target tissue of the host (Andras et al. 2020). Extensive attachment testing with a wide range of host and parasite isolates has shown that susceptibility is almost perfectly correlated with attachment, with little to no variation due to environmental or host condition (Duneau et al. 2011).

Previous studies have shown that *D. magna* resistance to *P. ramosa* attachment is governed by multiple epistatically interacting loci distributed across the *D. magna* genome. Genetic crosses of *D. magna* clones with differing *P. ramosa* resistance phenotypes have thus far identified six resistance loci: the A, B, C, D, E, and F loci. The A, B, and C loci cluster tightly together on chromosome 4 to form the ABC supergene, which shows major structural polymorphism between haplotypes, including long stretches of nonhomologous sequences that appear to be non-recombining (Bento et al. 2017). The F locus is closely located to the ABC cluster, while the D and the E loci are distributed elsewhere across the *D. magna*

genome, but epistatic interactions between combinations of these loci have been described (Bento et al. 2017; Ameline et al. 2021).

The loci which govern infection in the *P. ramosa* genome are less well understood, but there are indications that a highly expanded family of genes encoding collagen-like proteins may be a determinant of infection outcome. Collagen-like proteins are known to be strongly tied to the infection process in a number of bacteria species by mediating attachment to host cells (Qiu et al. 2021). Pasteuria collagen-like (PCL) genes are widely distributed across the *P. ramosa* genome in triplet clusters, potentially the consequence of repeated duplications of a highly mobile transposable element (McElroy et al. 2011). A previous study found that variation at one of these PCLs correlated perfectly with the ability of certain *P. ramosa* isolates to infect a specific *D. magna* genotype (Andras et al. 2020). Given that *P. ramosa* spores are coated with a thick layer of fibers hypothesized by be composed of collagen-like proteins (Andras et al. 2020), and that spore attachment to any of several sites on the host cuticle appears to be the primary determinant of infection outcome (Duneau et al. 2011; Fredericksen et al. 2021), these PCL genes are promising candidates for sites of interlinkage with host resistance genes.

Previous studies of the *D. magna* / *P. ramosa* system have examined loci governing the infection process through experimental contexts which allow for genomic variation only for the host or for the parasite. Although multiple resistance genes in the host and one infectivity gene in the parasite are known, the manner in which these genes interact with each other is not yet understood. Such interactions are at the core of matching-allele and gene-for-gene models, thus forming the most fundamental aspect of coevolutionary dynamics. A number of different statistical approaches have been developed to detect signals of coevolution, both at the genomic level, and the phylogenetic level (Legendre et al. 2002; Carlson et al. 2008; Wang et al. 2018; Märkle et al. 2021). The co-GWAS approach is an extension of single-phenotype GWAS (Genome Wide Association Study), which simultaneously considers genetic information from host and parasite. Through the combination of clinical data and genome-scale SNP arrays, co-GWAS has been used to identify genomic variants of clinical significance for HIV infection (Bartha et al. 2013), Hepatitis C (Ansari et al. 2017), and pneumococcal meningitis (Lees et al. 2019). In order to identify potentially interlinked loci among our system, we conducted a co-genome wide association study (co-GWAS) using wild collected *D. magna* and their naturally associated *P. ramosa* parasites.

RESULTS

Sequencing and mapping

We sequenced 258 *D. magna* naturally infected with *P. ramosa* collected during an epidemic across one season from a single pond, and separated the resulting reads by mapping against reference genomes for the host and parasite. Overall rates of contamination were low for whole-organism sequencing, with 92.8 % (11.0 SD) of reads mapping to either the host or parasite genome (S1 Fig). Mean depth of coverage was 31.0 (SD = 13.0) for *D. magna* and 318 (SD = 217) for *P. ramosa*. This difference in mean coverage reflects the smaller genome size of the parasite, which is approximately 2 Mb versus the approximately 230 Mb host genome. Ten of the samples showed low coverage for either the host or parasite genome and were excluded from further analysis (S1 Fig).

Genomic variation

We identified 21,933 variant positions (SNPs, indels, and SNP/indel combinations) in the *P. ramosa* sequence data. These variants were filtered for base and mapping quality, excessive read depth, and bi-allelic status, resulting in 10,310 variant positions retained for downstream analysis. For the much larger *D. magna* genome, an initial call set of 4,142,757 variants was reduced to 2,211,993 after identical filtering parameters were applied. Population-wide nucleotide diversity (π) was 0.26 for *D. magna* with per sample missingness rates < 1 %. Estimates of genetic diversity within *P. ramosa* samples varied dramatically, likely reflecting that some hosts had been infected by multiple *P. ramosa* genotypes, while others were subject to single infections (Fig 1A). Eight samples were monomorphic at nearly all sites, thus indicating the presence of only a single haploid *P. ramosa* genotype. The remaining samples showed variable rates of *P. ramosa* polymorphism with extreme cases showing variation at up to 50 % of segregating sites, suggesting multiple infections by dissimilar genotypes (Fig 1A).

Population structure

We examined host and parasite samples for hidden population structure using principal component analysis (PCA) and Discriminant Analysis of Principle Components (DAPC). The *D. magna* samples showed no discernable population structure, matching our expectations for a sexually reproducing population contained within a small pond. The strongest principal component for *D. magna* explained 3.5 % of total genomic variation, with subsequent PCs

136 explaining incrementally smaller values (Fig 1E, F). K-means clustering based on genetic
137 distance showed the strongest support for a single *D. magna* cluster, which is readily
138 observable upon visual inspection of the PCA ordination (Fig 1E).
139
140 In contrast to the host, the majority of genomic variance for *P. ramosa* could be summarized
141 by the first two principal components, which together explained 77 % of total variance (Fig
142 1B). Visual inspection of the first two axes of the PCA ordination showed the *P. ramosa*
143 samples arranged as a triangular cloud with three distinct genomic clusters in the corners,
144 which we have labeled as *Alpha*, *Beta*, and *Gamma* (Fig 1B). Samples infected by multiple *P.*
145 *ramosa* genotypes (Fig 1A) were located between the clusters, primarily along the edges of
146 the triangle. K-means clustering based on genetic distance supported the division of single-
147 infection samples into the *Alpha*, *Beta*, *Gamma* clustering scheme, with the possibility for
148 further subdivision of the *Alpha* lineage into three sub-clusters (Fig 1B, 1C). Admixture
149 analysis of our *P. ramosa* samples with K=3 groups showed identical placement of samples
150 respective to the *Alpha*, *Beta*, and *Gamma* clustering scheme as derived from DAPC analysis
151 (S2 Fig). For the sake of clarity, we hereafter refer to the three *P. ramosa* genomic clusters as
152 "lineages" without reference to specific taxonomic rank.
153
154 The examination of further parasite principal components revealed a small degree of
155 relatively continuous within-lineage variation, potentially reflecting the process of
156 recombination within lineages (Fig 1C, S2). Recombination is not well understood in *P.*
157 *ramosa,* but we could observe its signature in the form of linkage disequilibrium dissolution
158 with distance across the *P. ramosa* genome (S3 Fig). Admixture analysis indicated strong
159 support for recombination within lineages, but much less between the three primary lineages
160 (S2 Fig). Therefore, the boundaries between sub-clusters should be understood as
161 approximation rather than the clear divisions that we observe between the discrete *Alpha*,
162 *Beta*, and *Gamma* lineages.
163
164 Population structure is an important consideration in GWAS modeling, and is often included
165 as a covariate in the form of principal components or a relatedness matrix (Zhou and
166 Stephens 2012; Chang et al. 2015). This paradigm can be extended to co-GWAS models
167 through inclusion of principal components from both the host and parasite (Ansari et al.
168 2017; Naret et al. 2018). However, several unique features of our system require careful
169 consideration regarding the treatment of population structure in a co-GWAS context. In this

170 study, the *D. magna* samples originated from a single population absent of geographic
171 subdivision (a small pond). Under this demographic scenario, the major principal components
172 are likely to represent local genomic features rather than genome-wide structure. The
173 inclusion of these PCs as covariates in co-GWAS model might therefore mask highly
174 differentiated loci which are potentially of biological interest from model results. This is even
175 more the case for the parasite, as the strong lineage structure that we found for *P. ramosa*
176 may be tightly linked to (or even derive from) the infection phenotype of the parasite. If so,
177 the top principal components for the parasite would represent a large portion of the
178 biologically relevant aspects of its interaction with the host. Correcting for population
179 structure might therefore mask the biological associations at the core of the interaction.
180
181 *Co-GWAS*
182 In consideration of these aspects, we have produced three hierarchically nested co-GWAS
183 models that examine host-parasite interlinkage under different assumptions regarding
184 population structure, dominance, and host-specificity. Model 1 assumes that potentially
185 cofounding demographic structure exists for both host and parasite, and thus the model
186 contains principal components from both as covariates. Model 2 assumes that parasite
187 population structure is a consequence of host-specificity, and thus the model contains
188 principal components for only the host. Model 3 assumes that the host population is
189 unstructured and omits all principal components, which greatly reduces the total number of
190 parameters estimated. Many other biologically reasonable model structures could also be
191 envisioned, but we found that these three models provided a good overall representation of
192 the parameter space. Potential effects of host allele dominance could be tested only in model
193 3, as model structures which included further covariates experienced convergence problems
194 due to model complexity. Given the large number of pairwise associations that are tested
195 under each model ($>10^9$) we have avoided setting a specific p-value threshold to assign
196 statistical significance to any particular model results. Rather, the strongest peaks from each
197 model were considered as candidate loci for phenotypic confirmation through laboratory-
198 based infection trials.
199
200 Our first co-GWAS model contained controls for host and parasite population structure, with
201 the top 10 principal components from the host (22 % total variance) and top 2 principal
202 components from the parasite (82 % total variance) as model covariates. The results from this
203 model showed a single strong peak in the daphnia genome located precisely at the location of

204 a well-characterized locus for *P. ramosa* resistance - the ABC locus (Table 1). The ABC
205 locus is considered a supergene (Bento et al. 2017), but we likely observe only the effect of
206 the C locus here because the A locus shows no variation in our study population, and the B
207 locus is nearly fixed for one allele (Ameline et al. 2021). Note that the A and B loci are not
208 globally fixed and show greater polymorphism in some populations (Luijckx et al. 2014;
209 Metzger et al. 2016; Bourgeois et al. 2021). This genomic region showed a strong signal of
210 interlinkage with a tightly clustered set of genes encoding triplets of collagen-like proteins in
211 the *P. ramosa* genome (Fig 2). This small region contains the densest concentration of
212 collagen-like genes in the *P. ramosa* genome, containing PCL triplets [9-10-11], [12-13-14],
213 and [36-37-38] (Fig 2, S4). A single, apparently intragenic, SNP on the right arm of
214 chromosome 5 of the host genome also appeared among the top results for this model (Fig 2,
215 Table 1), but the complete absence of neighboring variants with similar small p-values
216 indicates that this peak is relatively weak candidate (S5 Fig).
217
218 Our second co-GWAS model included covariates from the host only, thereby allowing
219 parasite populations structure to be incorporated into the genomic terms of the model. This
220 model showed the same C locus / PCL interlinkage observed in model 1, and a further strong
221 signal of interlinkage precisely at the location of the D locus for *P. ramosa* resistance (Fig 2).
222 The D locus appears to be tightly interlinked with a narrow genomic region containing the
223 PCL gene triplet [21-27-28] (Table 1). We also observed a single, apparently intragenic, host
224 SNP on chromosome 1 among the top results for this model. Like the isolated SNP observed
225 in model 1, the complete absence of neighboring variants with similar p-values suggest that
226 this peak is relatively weak candidate.
227
228 Our third co-GWAS model accounted for the fact that our host population is best represented
229 as a single well-mixed population, and further omitted all principal components for the host.
230 Model 3 also allowed for dominance effects in the host genotype, which could not be
231 incorporated in previous models due to convergence problems with the larger number of
232 parameters estimated. The strongest signatures of interlinkage in model 3 were again located
233 between previously-characterized pasteuria-resistance loci in the host genome and PCL gene
234 triplets in the parasite genome (Fig 2). The E locus region for *P. ramosa* resistance appeared
235 as one of the largest peaks in model 3, and showed strong interlinkage with PCL triplets [6-7-
236 8], and [36-37-38]. We also observed a strong signal of interlinkage between the D locus for
237 *P. ramosa* resistance and PCL [24-25-26]. The C and D loci showed clear associations with

PCL gene triplets as observed in the other co-GWAS models, but with a relatively lower magnitude than other peaks in model 3 (S6 Fig).

In addition to these known pasteuria-resistance loci, we observe a strong signature of interlinkage in model 3 at two previously-uncharacterized positions in the host genome. The largest of these peaks was found across a broad section of the right arm of chromosome 5, and was associated with PCL triplets [6-7-8], [21-27-28], [24-25-26], and [36-37-38]. The extreme width of this peak is unusual, and perhaps indicates some type of structural polymorphism. The second uncharacterized peak in model 3 occurred between a region on the left arm of host chromosome 7 and PCL triplet [15-16-17]. Neither of these loci have been previously observed to relate to *P. ramosa* resistance in laboratory experiments, but they appear here as strong candidates for further investigation based on the width of the peaks and their highly specific PCL triplet association.

Phenotypic confirmation

In order to assess the correspondence between host and parasite phenotype, we conducted a series of infection trials using clone lines established from our wild-collected daphnia and a panel of *P. ramosa* isolates. This panel was comprised of five laboratory-cultured *P. ramosa* isolates (C1, C19, P15, P20, and P21), which in various combinations reveal the phenotype of the known pasteuria-resistance loci (Luijckx et al. 2013; Bento et al. 2017; Bento et al. 2020; Ameline et al. 2021). For example, the allelic state at the *D. magna* C locus is defined in relation to susceptibility to *P. ramosa* isolates C1 and C19, with resistance being dominant (Bento et al. 2017). Three resistotypes comprised 81% our sequenced samples: [RRSRS] (52%), [SSSSS] (21%), and [RRSSS] (8%). These values match expectations from previous studies of the *P. ramosa* epidemic at lake Aegelsee which observed the same three resistotypes in roughly similar proportions (Ameline et al. 2021). Twelve additional rare resistotypes were observed with most present in only a single individual. With a much larger sample size Ameline et al. (2021) also observed that certain multi-locus resistotypes are rarely or never observed. We observed variation in respect to resistance/susceptibility for all tested isolates, although most daphnia (93%) were susceptible to isolate P15. Only one specimen showed resistance to all five laboratory isolates. It is interesting to note that the most common resistotypes were not necessarily those which conferred the broadest pattern of resistance.

272 We then applied DAPC clustering to the genomic regions corresponding to each of the
273 resistance loci, and grouped the genomic clusters by the relevant resistotype to define
274 functional genotype groups (S7, S8, S9 Tables). Up to 10 genotype clusters could be detected
275 at each resistance locus, likely representing several haplotypes in various combinations with
276 each other. Our goal was to identify the minimum number of clusters needed to differentiate
277 resistance phenotypes, and in all cases, we found that three clusters gave us the best
278 segregation of resistotypes. These three clusters could then be collapsed into two groups
279 representing primarily resistant or primarily susceptible phenotypes. This classification
280 scheme of three genotypes clusters segregating into two phenotypes likely reflects underlying
281 dominance effects in heterozygous loci as predicted by our genetic models, but the presence
282 of multiple haplotypes and uncertainty about the precise nature of the variants at these
283 resistance loci limits our inference. Among our samples we observed perfect correspondence
284 between DAPC genotype cluster at the C locus and resistance phenotype, with one of
285 genotypes (C') showing complete susceptibility to C1 and C19 and the other (C) showing
286 resistance to C1 and C19 (S6 Table). We observed only partial correspondence between
287 resistotype and genotype for the D and E loci. In both cases, one genotype cluster (D or E)
288 corresponded to exactly one resistance phenotype, but the alternative genotype cluster (D' or
289 E') corresponded to multiple resistance phenotypes (S7, S8 Table). This imperfect
290 correspondence between genotype and phenotype does not appear to be an artifact of our
291 clustering methodology or dominance effects, as apparently identical genotypes were
292 associated with multiple resistance phenotypes.
293
294 *Uncharacterized loci recovered from co-GWAS*
295 Our co-GWAS models recovered a strong signal of interlinkage at two previously
296 uncharacterized loci in the *D. magna* genome. The strongest of these peaks spanned a large
297 (~ 4 Mb) region on the right arm of chromosome 5, while the other spanned ~ 100 Kb on the
298 left arm of chromosome 7. Given the imperfect sorting of D and E locus genotypes into their
299 expected phenotypes, we hypothesized that one or both of these uncharacterized loci could
300 represent an unknown pasteuria-resistance locus that epistatically interacts with either locus.
301 We therefore performed a series of simple GWAS experiments to determine if these loci
302 correspond to different pasteuria resistance phenotypes. We discovered that the candidate
303 locus on the right arm of chromosome 5 is strongly associated with the resistotype RRS
304 relative to the *P. ramosa* isolates C1, C19, and P20 (Fig 3). This is the canonical resistotype
305 used to identify the allelic state at the E locus in laboratory-based experiments (Ameline et al.

306 2021), and provides further evidence that this previously uncharacterized locus may
307 epistatically interact with other loci to affect resistance phenotype. We could not identify a
308 similar correlation between resistance phenotype and the second uncharacterized locus on
309 chromosome 7, but future experiments are planned to further examine this possibility through
310 an expanded panel of *P. ramosa* isolates.
311
312 *Genotype – Genotype matrix*
313 Host specificity in the *D. magna* / *P. ramosa* system is hypothesized to arise from relatively
314 simple host-parasite infection matrices, such as a matching allele matrix, but the presence of
315 multiple interacting loci in both host and parasite genomes has the potential to yield
316 considerable complexity. Nonetheless, our functional grouping of hosts according to
317 resistance locus genotypes revealed strong associations with the parasite genomic clusters.
318 Chi-squared tests of genotype contingency tables showed significant associations for the C
319 locus ($X^2 = 16.4$, $p = 2.5^{-3}$), D locus ($X^2 = 32.5$, p-value = 1.5^{-6}), and E locus ($X^2 = 55.2$, p =
320 3.0^{-11}), with deviations from expected values resembling a matching allele model (Fig 4). For
321 example, we observed that *D. magna* carrying the D genotype were most likely to be infected
322 by parasites from the *Gamma* lineage, but apparently immune to infection by *Gamma* when
323 carrying the D' genotype (Fig 4). Similarly, the E genotype appears to confer strong
324 resistance to the *Beta* lineage, while the alternative E' genotype confers strong susceptibility.
325 This specificity remains observable at finer scales, with various sub-clusters of the *Alpha*
326 lineage showing strong differences in ability to infect different C and D locus genotypes.
327
328 **DISCUSSION**
329
330 *Summary*
331 Our results showed a clear signal of genomic interlinkage between several loci in the *D.*
332 *magna* genome and a set of genes encoding for collagen-like protein in *P. ramosa.* Our
333 findings were supported by our *P. ramosa* attachment assays, which showed a strong
334 correspondence between phenotype and genotype at the recovered resistance loci. The fact
335 that our co-GWAS model recovered all known resistance loci of daphnia that segregate in our
336 study population stands as a strong biological validation of our results, as experiments
337 describing these loci employed genetic crosses and phenotyping experiments using a
338 laboratory-based panel of hosts and parasites (Metzger et al. 2016; Bento et al. 2017; Bento et
339 al. 2020; Ameline et al. 2021). Our co-GWAS models recovered these loci using only

340 genomic data from wild-collected specimens, with phenotypic data employed only for post-
341 hoc confirmation. While most of these loci in the host were known previously, their
342 interactions with infectivity loci in the parasite were entirely unknown. Our experiments
343 revealed that these are not general resistance and infectivity loci, but rather their effect is
344 contingent on the allelic state at interacting loci in the host or parasite. We also identified a
345 new candidate locus for pasteuria-resistance in the host genome which strongly correlates
346 with resistance to *P. ramosa* isolate P20. A further important finding is that collagen-like
347 gene triplets in the *P. ramosa* genome (but not single collagen-like genes) are key
348 determinants of infectivity. These new candidate loci for infectivity and resistance will be
349 examined through future experiments with genetic crosses and QTL mapping.
350
351 *Co-GWAS model differences*
352 Our co-GWAS modeling revealed that different assumptions regarding population structure,
353 dominance, sample relatedness, and other factors yielded important differences in the results.
354 Therefore, we present not a single model that shows only a snapshot of this parameter space,
355 but present three co-GWAS models which covers the range of variation that we observe
356 under a range of biologically reasonable assumptions. Our first co-GWAS model includes
357 principal components from both the host and parasite as covariates. As parasite lineage
358 structure is strongly correlated with the first two principal components of the *P. ramosa*
359 genome, we primarily observed the effects of within-lineage variation in model 1. This is
360 supported by our host genotype – parasite lineage association tables (Fig 4) which show that
361 the effect of the host's C locus is most apparent across sub-groups within the *Alpha* lineage.
362
363 Our second co-GWAS model includes covariates from the host only, thereby allowing
364 parasite populations structure to be incorporated into the genomic terms of the model. This
365 approach could be considered an analytical mistake, as it could increase the rate of false
366 positives due to non-adaptive demographic effects such as co-dispersal of host and parasite
367 (Naret et al. 2018). However, under such a scenario all lineage specific alleles would show an
368 equally strong association. We do not observe this phenomenon in our results for model 2,
369 rather we observe clearly distinct peaks at specific regions of the host and parasite genome
370 which contain genes previously hypothesized to govern the infection process. Model 2
371 reflects the hypothesis that population structure in *P. ramosa* is a direct result of genetic
372 interactions with its host rather than a confounding factor.
373

374 Our third co-GWAS omitted host and parasite population structure under the assumption that
375 specific combinations of host and parasite genomes occur due to biological rather than
376 demographic reasons. This assumption is reasonable given that all samples were collected
377 from one population during one season, but would be advised against when populations are
378 comprised of discrete demes or drawn from a wide geographic range. Model 3 also allowed
379 for dominance effects in the host genotype, which could not be incorporated in the models 1
380 and 2 due to convergence issues arising from the larger number of parameters. In this model
381 we observed strong peaks of interlinkage between pasteuria-resistance loci and PCL gene
382 triplets, and identified two additional candidate loci in the host genome showing similar
383 signals of interlinkage. Subsequent laboratory experiments showed one of these loci to be
384 highly correlated with resistance to *P. ramosa* isolate P20.
385
386 Although each of these models vary to some degree in specific details, we observe a
387 consistent pattern of pasteuria-resistance genes in the host showing a highly specific
388 association with collagen-like genes in the *P. ramosa* genome that are arranged in a
389 conserved triplet configuration. The major differences between these models can be readily
390 interpreted, and to some degree, predicted by the biology of the system. As the E locus loads
391 heavily on the top principal components of *D. magna* in our study population (S11 Fig), we
392 expect that the effect of this locus should detectable only in model 3. Similarly, model 1 is
393 constrained in such a manner that only within-lineage associations should be observable,
394 which is exactly what the model shows. The C and D loci remain detectable in model 3 (S6,
395 S12 Fig), but show a much weaker signal than the E locus, reflecting previous observations
396 that the E locus appears to be the primary determinant of pasteuria resistance in our study
397 population (Ameline et al. 2021; Ameline et al. 2022).
398
399 *Discovery of P. ramosa lineages*
400 Our discovery of three distinct evolutionary lineages of *P. ramosa* within the study site was a
401 particularly unexpected result of this project. Although most daphnia hosts were infected by
402 only a single lineage of pasteuria, simultaneous infection by multiple lineages of pasteuria
403 were observed. Given that we detected strong evidence for recombination within our study
404 population (S2, S3 Fig), a presently unknown mechanism is clearly maintaining some form of
405 reproductive isolation between these lineages. The nature of this reproductive isolation
406 between pasteuria lineages is an important question for further investigation. We intend to
407 conduct broader surveys of pasteuria populations to determine if additional lineages occur

408 globally. The discovery that *P. ramosa* isolates arise from discrete evolutionary lineages also
409 allows us to assess how well our laboratory panel represents the diversity of genotypes
410 present at our study site. Preliminary evidence with newly developed genetic markers
411 indicates that the isolates C1, C19, and P20 belong to the *Beta* lineage, the isolates P15 and
412 P21 belong to the *Gamma* lineage, and that the *Alpha* lineage is not represented in our
413 standard panel. We are in the process of developing several new pasteuria cultures from the
414 *Alpha* lineage to deploy in future studies, and a panel of genetic markers to differentiate
415 lineages and potential sub-lineages.
416
417 *Signatures of balancing selection at interlinked loci*
418 Negative-frequency dependent selection is a form of balancing selection that is expected to
419 yield a genomic signature of locally elevated nucleotide diversity at the sites under selection
420 (Ebert and Fields 2020). This pattern arises because common host variants are selected
421 against by parasite variants that specialize on these host variants. A previous study of the
422 genetic basis of *P. ramosa* infection found usually high levels of genetic diversity at a
423 number of PCL genes, which the authors interpreted as evidence of balancing selection at
424 those loci (Andras et al. 2018). Samples for this previous study were drawn from a wide
425 geographic range that spanned across the Western Palaearctic. Despite the fact that our study
426 samples were drawn from a single population, we observed peaks in nucleotide diversity at
427 the same genomic positions (Fig 2). In respect to the *D. magna* host, we observed the highest
428 levels of nucleotide diversity at the position of the ABC locus, which is known to contain
429 major structural variants of sufficient divergence to limit recombination (Bourgeois et al.
430 2021). Thus, we observe evidence for balancing selection in terms of nucleotide diversity as
431 well as genomic structural diversity among both the host and parasite dimensions of this
432 system.
433
434 *Molecular mechanisms of infection and resistance*
435 Pasteuria collagen-like proteins (PCLs) belong to a larger class of collagen-like proteins
436 which are known to occur in at least 14 bacterial phyla (Qiu et al. 2021). For example, many
437 species of pathogenic *Streptococcus* contain collagen like proteins (Xu et al. 2002; Karlström
438 et al. 2004; Paterson et al. 2008; Lukomski et al. 2017), as does the highly virulent *Bacillus*
439 *anthracis* (Henriques and Moran 2007). Collagen-like proteins have been directly linked to
440 infectivity in the gut pathogen *Clostridium difficile* (Strong et al. 2014), drug resistant strains
441 of the human and livestock parasites *Burkholderia* sp. (Bachert et al. 2015), and the causative

agent of Legionnaire's disease, *Legionella pneumophila* (Vandersmissen et al. 2010). Collagen-like proteins are hypothesized to mediate the infection process through the mechanism of attachment to host tissues (Qiu et al. 2021). Compared to other bacterial species, *P. ramosa* has an unusually large number of collagen-like proteins, with nearly 50 genes identified thus far (McElroy et al. 2011). The enormous repertoire of collagen-like proteins in *P. ramosa* could be explained as a long-term effect of balancing selection due to a tight coevolutionary history with its host. A noteworthy finding is that the collagen-like genes revealed by our co-GWAS models all appeared in a specific triplet formation. The *P. ramosa* genome contains many isolated collagen genes and loose aggregations of collagen genes, but none of these showed strong association with the host. Thus, with regard to infection phenotype, we observed that not only the nature of the gene is important, but also the spatial orientation of the gene in the genome. The function of the collagen-like gene triplets, as opposed to single genes is not known.

The molecular mechanisms which determine *D. magna* resistance to specific *P. ramosa* genotypes are not yet resolved, although a promising hypothesis concerns the post-translational modification of cuticle proteins via the attachment of branching sugars (*i.e.,* glycosylation). Previous studies have found major differences between susceptible and resistant clones at the ABC locus in regards to genes encoding fucosyltransferases, glucosyltransferases, galactosyltrasferases – all of which are involved in the post-translational attachment of sugars to proteins (Bento et al. 2017). The E locus, which appears have an independent evolutionary origin from the ABC locus, seems to be enriched for galactosyltransferase and glucosyltransferase genes as well (Ameline et al. 2021). In an interesting parallel, it has been proposed that glycosylation of amino acid residues at the C-terminal domain also plays an important role in attachment specificity of bacterial collagen-like proteins (Strong et al. 2014; Qiu et al. 2021). There is some support for this hypothesis from a previous study of *P. ramosa* infectiousness, which found that a predicted N-glycosylation site in the C-terminal domain of PCL 7 correlated perfectly with infection phenotype (Andras et al. 2020).

Functional testing of resistance loci

Phenotypic assessment of resistance loci via pasteuria attachment assays has provided important context and support for our co-GWAS model results in several ways. First, it allowed us to test whether any of the uncharacterized peaks in our models corresponded to an

identifiable resistance phenotype. The strongest peak recovered across any of our models was localized to the right arm of chromosome 5 in the *D. magna* genome, a position which has not been previously associated with pasteuria resistance. Our functional testing revealed that this genomic region is strongly associated with resistance to pasteuria isolate P20, and thus very likely contains uncharacterized resistance genes. Secondarily, the genomic positions and genetic models for pasteuria resistance were mostly developed through laboratory crosses of *D. magna* from other populations. Functional testing allowed us to verify that pasteuria resistance in a wild population conformed to the patterns expected by our genetic models. Third, functional testing allowed us to determine how many DAPC clusters were necessary to differentiate resistance phenotypes. The imperfect segregation of resistotypes according to our DAPC clusters for the D and E loci show an unexpected departure from the current genetic models of pasteuria resistance, and indicates the possible influence of a yet unknown interacting resistance locus, perhaps one of the uncharacterized loci recovered from our co-GWAS models.

Generalization of co-GWAS and extension to other systems

The strength of our co-GWAS results are in some part due to the highly specific nature of the interaction between *D. magna* and *P. ramosa*, with specific genotype combinations showing either complete resistance or complete susceptibility to infection. This degree of specificity has allowed us to resolve interlinked host and parasite loci using a relatively modest sample of 258 individuals, which is considerably fewer than typically required to resolve traits of a more continuous nature using conventional GWAS approaches. In general, we expect that the detection power of a co-GWAS is constrained in the same manner as a conventional GWAS; Reasonable detection power will require relatively larger sample sizes in cases where there is low heritability of the trait of interest, complex genomic architectures, or polygenic contributions to a single trait (Korte and Farlow 2013). In the specific context of co-GWAS one should also expect that sample sizes will need to increase as the specificity of the interaction decreases.

Regarding the issue of epistasis in co-GWAS (or GWAS more generally), our study shows that epistatic interactions can be resolved without explicitly providing prior knowledge of epistatic interactions. Our co-GWAS successfully recovered the E-locus for pasteuria resistance, despite the fact that the phenotype encoded by the E-locus is contingent upon the allelic state at the dominant C locus (Fredericksen et al. 2021). While our models did not

510 recover the signal of the A and B loci, which share a similar epistatic relation with the C
511 locus, the underlying issue is more likely a lack of genetic variants rather than insufficiency
512 of the model itself as these loci appear to be nearly fixed in our study population (Ameline et
513 al. 2021).
514
515 In conclusion, understanding the genomic basis of infectious disease is a fundamental
516 objective in the study of coevolution. Our results show a clear signal of interspecies linkage
517 disequilibrium across multiple sets of interacting loci in a naturally coevolving system, thus
518 confirming the most fundamental assumption of host-parasite coevolution. Previous co-
519 genomic association studies have identified variants of clinical significance for HIV
520 infections (Bartha et al. 2013), Hepatitis C (Ansari et al. 2017), pneumococcal meningitis
521 (*16*), and malaria (Band et al. 2021) through a combination of SNP arrays and patient clinical
522 data. Our approach moves a step further by examining the complete genomes of naturally
523 infected hosts and parasites from a host population with a known history of parasite
524 epidemics. Our central finding is an underlying host-parasite genetic interaction matrix, as
525 such matrices are at the core of coevolutionary theory, and their topology determines the
526 tempo and mode of coevolution. Our matrix confirms the importance of multiple loci in both
527 antagonists, acting together within and across genomes, with epistasis playing a decisive role
528 for the host and the parasite. We demonstrate that the co-genomic framework can be
529 successfully applied to non-model systems, and given sufficiently strong host-parasite
530 specificity, resolution of complex traits is possible in a candidate-free manner. In the future,
531 this method will be useful to elucidate other types of pairwise interactions, such as
532 commensalism, mutualism, predation, and assortative mating in the context of sexual
533 selection.
534
535 **MATERIALS AND METHODS**
536
537 *Field Collections*
538 We collected *D. magna* samples from Lake Aegelsee (47.558048, 8.861063) via horizontal
539 net tows at the deepest place during a strong *P. ramosa* epidemic in summer 2019. These
540 wild-collected daphnia were monitored in the laboratory for signs of *P. ramosa* infection and
541 the appearance of offspring. Although *P. ramosa* typically castrates the host, clonal
542 reproduction is still possible in the early stages of infection. As *P. ramosa* is exclusively
543 transmitted through the environment, the laboratory lines were quickly separated from the

544 mother and remained uninfected throughout the experiment. After verifying *P. ramosa*
545 infection status and establishing healthy clonal lines, we preserved the original wild-collected
546 individuals in 90 % EtOH at -20 °C for later DNA extraction.
547
548 *DNA extraction and Sequencing*
549 Whole-organism DNA extractions from daphnia may contain a high proportion of non-target
550 DNA from undigested food, gut microbiota, and bacteria microfilm on the cuticle. To reduce
551 contaminants, we cleared the gut by feeding the daphnia with a suspension of sterile beads
552 (Sephadex G-25, cross-linked dextran gel) three times per day for at least 24 hours. After the
553 gut was visibly cleared of food, we monitored containers with individual daphnia every 2-4
554 hours for the presence of a molted cuticle. After molting, daphnia were immediately
555 preserved in 90 % EtOH at -20 °C for later DNA extraction, sharply reducing the amount of
556 bacterial contamination in the preserved sample. Preliminary experiments showed this
557 protocol to be effective in limiting the amount of non-target DNA in preserved samples to
558 less than 5 %.
559
560 We extracted DNA from infected daphnia using a modified protocol for a Gentra PureGene
561 column-based extraction kit. Briefly, we homogenized whole daphnia with a pestle and
562 incubated the samples overnight at 55 °C in a solution of lysis buffer and Proteinase K. The
563 samples were then incubated for 30 minutes at 37 °C with RNase A, treated with a protein
564 precipitation solution, and centrifuged to remove precipitates. The supernatant was then
565 subject to a chilled isopropanol precipitation with glycogen added as a DNA carrier. The
566 DNA pellet was then resuspended in a buffer solution and stored at -20 °C. Our complete
567 extraction protocol is available on the GitHub repository for this manuscript
568 (https://github.com/edexter/Interlink).
569
570 We then prepared genomic libraries for short-read sequencing using a NEBNext Ultra II
571 DNA Library Prep Kit for Illumina. The libraries were sequenced across multiple runs of a
572 Novaseq 6000 to generate paired-end 150 bp reads, aiming for at least 30X coverage across
573 host and parasite genomes. Samples were sequenced with individual barcodes for subsequent
574 demultiplexing and inspection for sequencer batch and lane effects. Genomic library
575 preparation and Illumina sequencing were performed at the Basel Genomics Facility, Basel,
576 Switzerland.
577

578 *Host phenotyping*
579 The most important step of the *P. ramosa / D. magna* infection process is attachment of *P.*
580 *ramosa* spores to the any of several sites on the cuticle, and may occur through the uptake of
581 *P. ramosa* spores during feeding (Duneau et al. 2011; Fredericksen et al. 2021). Attachment
582 is a necessary requirement for successful infection and variation in attachment explains the
583 vast majority of overall infection success (Hall et al. 2019, Molecular Ecology). Attachment
584 specificity between host and parasite genotype combinations can be determined via a
585 relatively simple attachment test using fluorescently labeled pasteuria spores. Experimental
586 studies based upon this attachment test have found a nearly perfect correlation between
587 attachment and infection outcome, with little to no effect of environmental or host condition
588 (Duneau et al. 2011).
589
590 We collected resistance phenotype data of the host (aka. "resistotype") for a subset of 107
591 genotypes of our sequenced *D. magna* clones, with each clone tested in triplicate. Daphnia
592 resistotype was assessed through gut attachment tests with fluorescently labeled pasteuria
593 spores using a standardized panel of five pasteuria isolates: C1, C19, P15, P20, and P21
594 (Duneau et al. 2011; Bento et al. 2017; Bento et al. 2020; Ameline et al. 2021). Resistance
595 (R) or susceptibility (S) to each isolate is denoted in a five-letter resistotype code with each
596 position corresponding to a single isolate. For example, the resistotype [SRRRR] would
597 indicate susceptibility only to C1, while the resistotype [SSSRR] would indicate
598 susceptibility to C1, C19, and P15. These attachment data were used for *post hoc* validation
599 of our co-GWAS results through comparison of genotypes at interlinked loci and resistance
600 phenotypes.
601
602 *Bioinformatics*
603 De-multiplexed sequence-read pairs were trimmed to remove low-quality reads and adaptor
604 sequences using Trimmomatic version 0.39 (Bolger et al. 2014). Duplicate reads were then
605 removed using Picard version 2.9.2. The trimmed reads were mapped against host and
606 parasite reference genomes using BWA-MEM version 0.7.15 operating under default
607 parameters (Li 2013). Reads were mapped to the daphnia XINB version 3.0 draft genome
608 assembly and the pasteuria isolate C1 version 1.0 draft genome assembly (manuscripts in
609 prep. – available by request). Reads mapping to both host and parasite genome were flagged
610 for downstream filtering. We jointly called genomic variants (SNPs, indels, and mixed-type
611 variants) across all samples using the GATK haplotype caller following the best practices

612 pipeline for diploid samples (Auwera and O'Connor 2020). Although *P. ramosa* is haploid,
613 this approach enabled us to differentiate single genotype infections from multiple infections,
614 and to identify major and minor alleles within each pool. *In silico* experiments showed little
615 change in the major/minor alleles identified when calling *P. ramosa* variants under different
616 ploidy models.
617
618 The host and parasite VCF files were filtered to remove low-quality bases, poor alignment
619 scores, or extreme strand biases. Variants were then filtered to exclude sites with excessive
620 depth (> 2x mean depth), or excessive instances of dual mapping (reads mapping to both
621 genomes) using a custom R script. Based upon visual inspection of dual mapping regions,
622 low-complexity sequences rather than assembly errors or gene homology appear to be the
623 most likely cause of dual mapping. The VCF files were then filtered to remove multi-allelic
624 variants and converted to PED files for input to Plink for co-GWAS analysis. Summary
625 statistics related to read mapping were calculated with SAMtools version 1.10 (Li et al.
626 2009). We calculated nucleotide diversity (π) for host and parasite genomes with VCFtools
627 version 0.1.16 (Danecek et al. 2011). For the host, we calculated π across 100 Kb sliding
628 windows with a 1 Kb offset. Across the much smaller parasite genome, we calculated π
629 across 500 bp sliding windows with a 250 bp offset. Precise filter cutoff values and other
630 parameters can be found along with our complete code at the associated Github repository.
631
632 *Co-GWAS analysis*
633 We employed a co-genome wide sequencing association study (co-GWAS) framework to
634 search for interlinked genomic regions of the host and parasite. This approach is based on the
635 regression of host genotypes against parasite genotypes for every pairwise combination of
636 loci. Similar methods of genome-to-genome association testing have been previously
637 employed to find clinically relevant variants in HIV (Bartha et al. 2013), Hepatitis C (Ansari
638 et al. 2017), *Streptococcus pneumoniae* (Lees et al. 2019), and *Plasmodium falciparum* (Band
639 et al. 2021) using human SNP array data. We prepared our genomic data for co-GWAS by
640 removing variants with a minor allele frequency less than 0.05 or missingness greater than
641 0.20. Pairwise relatedness was calculated for the host using the KING kinship estimator, and
642 samples showing relatedness greater than 0.35 (possible clone mates) were thinned to remove
643 redundant samples. To reduce the probability of false positives due to population structure,
644 we conducted PCA on subsets of linkage disequilibrium thinned loci for both host and
645 parasite. Loci were thinned using the indep-pairwise function in Plink with a maximum r2

646 threshold of 0.2 across a 1 kb (pasteuria) or 1000 kb (daphnia) sliding window. A smaller
647 window size was selected for the parasite due to its relatively small genome. The top
648 principal components were then included as covariates in our co-GWAS models. We used
649 Plink version 2.00a3LM for PCA, frequency-based filtering, and co-GWAS analysis (Chang
650 et al. 2015).
651
652 Our GWAS analysis was structured as a logistic regression model of the form:
653
654 $$Y_{ij} \sim \mathbf{X}k + \mathbf{Z} + e$$
655 Where *Y* is a binary variable [0,1] indicating the presence or absence of allele *i* at locus *j* in
656 the parasite genome. For example, the biallelic SNP A/T would be split into 2 variables. A
657 pasteuria sample containing only at the A allele would be coded as 1 for the first variable and
658 0 for the second, a pasteuria sample showing only the T allele would be coded as 0 and 1
659 respectively, and a multiple infected sample showing both alleles (i.e. a heterozygote
660 genotype call) would be coded as 1 and 1. The variable *X* represents the genotype at locus *k*
661 in the host genome expressed as the major allele dosage [0,1,2], a dominant reference allele
662 model [1,1,0], or a dominant alternate allele model [0,1,1]. These different coding schemes
663 reflect the fact that host samples contain a single diploid individual while their infecting
664 parasites may contain a pool of haploid individuals (i.e., multiple infections). Note that
665 although dominance models are more biological plausible than a simple genotypic dosage
666 model, they are rarely employed in the context of GWAS due to statistical difficulties in
667 detecting non-additivity (i.e., too few homozygous-minor genotypes) (Chang et al. 2015;
668 Marees et al. 2018). The term *Z* [0-1] represents a matrix of the top *n* principal components
669 and controls for population structure among samples, with permutations of our primary co-
670 GWAS model containing different subsets of principal components. In order to reduce the
671 computational burden of weak or non-significant associations, test results with p-values
672 greater than 10^{-4} were not stored for downstream analysis or plotting. This cutoff was derived
673 from preliminary co-GWAS trials which showed that p-values below this threshold were
674 uniformly distributed across the daphnia genome and generally uninformative.
675
676 Because each variant position in the host genome is tested against each variant position in the
677 parasite genome, co-GWAS analysis can generate a considerable number of false positives
678 purely through stochastic processes. Rather than applying a simple threshold to denote
679 statistical significance, we utilized information about the magnitude and breadth of each peak

680 to create a list of candidate loci for further examination. Specifically, biologically relevant
681 associations are expected to yield a broad peak of elevated p-values, including nearby
682 flanking regions which rapidly decay with distance from the site of selection. This pattern is a
683 characteristic signature of linkage disequilibrium decay due to recombination and provides a
684 useful biological validation to our statistical results. In contrast, we expect that associations
685 due to mapping errors or stochastic sampling effects will result in isolated peaks comprised
686 by one or very few variants.
687
688 *Host and parasite genotype clustering*
689 We extracted the sequence data from the genomic region corresponding to each of the known
690 host resistance loci and applied a discriminant analysis of principal components (DAPC)
691 function to aggregate individual genotypes into clusters of broadly similar genotypes
692 (Jombart et al. 2010). Genotype clusters were then grouped by resistance phenotype to define
693 functional groups. Each host was assigned a set of three resistance locus codes denoting the
694 functional group of the C, D, and E locus, each with two functional groups (e.g., C vs C'). We
695 applied the same DAPC method to our parasite samples, using the entire parasite genome
696 rather than individual loci. DAPC and PCA were performed using the Adegenet version 2.1.3
697 package for R version 4.0.4 (Jombart 2008). All statistical analyses were performed using R
698 unless specifically mentioned otherwise, and all figures were produced using the ggplot2
699 (version 3.3.3) package (R Core Team 2016; Wickham et al. 2018). DAPC clustering results
700 were compared against genomic clusters generated via the K-means cross-validation
701 algorithm implemented in Admixture version 1.3.0 (Alexander et al. 2009). Admixture
702 analysis was performed using a set of LD-thinned biallelic variants from singly-infected
703 samples, with cross validation set to select the optimal value for K ranging from 1 to 10.

Acknowledgments

We would like to thank the Ebert lab members for valuable discussions and suggestions.

Funding

This work was supported by the European Commission Marie Curie Postdoctoral Fellowship grant #835379 (ED, DE) and the Swiss National Science Foundation (SNSF) grant #310030_188887 (DE)

Author contributions:

Conceptualization: ED, DE, PDF
Methodology: ED, DE, PDF
Investigation: ED, DE
Visualization: ED
Funding acquisition: ED, DE
Project administration: ED, DE
Supervision: DE
Writing – original draft: ED, DE
Writing – review & editing: ED, DE, PDF

Competing interests

Authors declare that they have no competing interests

Data and materials availability

The complete annotated code necessary to reproduce all analyses and figures presented here is available on GitHub (https://github.com/edexter/Interlink). The raw genomic data pertaining to this study are available from the NCBI Short Read Archive (SRA) (accession number in progress).

732 **REFERENCES**

733 Agrawal A, Lively CM. 2002. Infection genetics: gene-for-gene versus matching alleles models and all
734 points in between. *Evol. Ecol. Res.* 4:91–107.

735 Alexander DH, Novembre J, Lange K. 2009. Fast model-based estimation of ancestry in unrelated
736 individuals. *Genome Res.* 19:1655–1664.

737 Ameline C, Bourgeois Y, Vögtli F, Savola E, Andras J, Engelstädter J, Ebert D. 2021. A two-locus
738 system with strong epistasis underlies rapid parasite-mediated evolution of host resistance.
739 *Mol. Biol. Evol.* 38:1512–1528.

740 Ameline C, Voegtli F, Andras J, Dexter E, Engelstädter J, Ebert D. 2022. Genetic slippage after sex
741 maintains diversity for parasite resistance in a natural host population. *Sci. Adv.* 8:eabn0051.

742 Andras JP, Fields PD, Du Pasquier L, Fredericksen M, Ebert D. 2020. Genome-wide association
743 analysis identifies a genetic basis of infectivity in a model bacterial pathogen. *Mol. Biol. Evol.*
744 37:3439–3452.

745 Andras JP, Fields PD, Ebert D. 2018. Spatial population genetic structure of a bacterial parasite in
746 close coevolution with its host. *Mol. Ecol.* 27:1371–1384.

747 Ansari MA, Pedergnana V, Ip CLC, Magri A, Von Delft A, Bonsall D, Chaturvedi N, Bartha I, Smith D,
748 Nicholson G, et al. 2017. Genome-to-genome analysis highlights the effect of the human
749 innate and adaptive immune systems on the hepatitis C virus. *Nat. Genet.* 49:666–673.

750 Auwera GAV der, O'Connor BD. 2020. Genomics in the Cloud: Using Docker, GATK, and WDL in Terra.
751 O'Reilly Media, Inc.

752 Bachert BA, Choi SJ, Snyder AK, Rio RVM, Durney BC, Holland LA, Amemiya K, Welkos SL, Bozue JA,
753 Cote CK, et al. 2015. A unique set of the Burkholderia collagen-like proteins provides insight
754 into pathogenesis, genome evolution and niche adaptation, and infection detection. *PLOS*
755 *ONE* 10:e0137578.

756 Band G, Leffler EM, Jallow M, Sisay-Joof F, Ndila CM, Macharia AW, Hubbart C, Jeffreys AE, Rowlands
757 K, Nguyen T, et al. 2021. Malaria protection due to sickle haemoglobin depends on parasite
758 genotype. *Nature*:1–9.

759 Bartha I, Carlson JM, Brumme CJ, McLaren PJ, Brumme ZL, John M, Haas DW, Martinez-Picado J,
760 Dalmau J, López-Galíndez C, et al. 2013. A genome-to-genome analysis of associations
761 between human genetic variation, HIV-1 sequence diversity, and viral control. *eLife*
762 2:e01123.

763 Bento G, Fields PD, Duneau D, Ebert D. 2020. An alternative route of bacterial infection associated
764 with a novel resistance locus in the Daphnia–Pasteuria host–parasite system. *Heredity*
765 125:173–183.

766 Bento G, Routtu J, Fields PD, Bourgeois Y, Pasquier LD, Ebert D. 2017. The genetic basis of resistance
767 and matching-allele interactions of a host-parasite system: The Daphnia magna-Pasteuria
768 ramosa model. *PLOS Genet.* 13:e1006596.

769 Bolger AM, Lohse M, Usadel B. 2014. Trimmomatic: a flexible trimmer for Illumina sequence data.
770 *Bioinformatics* 30:2114–2120.

771 Bourgeois Y, Fields PD, Bento G, Ebert D. 2021. Balancing Selection for Pathogen Resistance Reveals
772 an Intercontinental Signature of Red Queen Coevolution. *Mol. Biol. Evol.* 38:4918–4933.

773 Carlson JM, Brumme ZL, Rousseau CM, Brumme CJ, Matthews P, Kadie C, Mullins JI, Walker BD,
774 Harrigan PR, Goulder PJR, et al. 2008. Phylogenetic dependency networks: Inferring patterns
775 of CTL escape and codon covariation in HIV-1 Gag. *PLoS Comput. Biol.* 4.

776 Chang CC, Chow CC, Tellier LC, Vattikuti S, Purcell SM, Lee JJ. 2015. Second-generation PLINK: rising
777 to the challenge of larger and richer datasets. *GigaScience* 4:s13742-015-0047–0048.

778 Danecek P, Auton A, Abecasis G, Albers CA, Banks E, DePristo MA, Handsaker RE, Lunter G, Marth
779 GT, Sherry ST, et al. 2011. The variant call format and VCFtools. *Bioinformatics* 27:2156–
780 2158.

781 Duneau D, Luijckx P, Ben-Ami F, Laforsch C, Ebert D. 2011. Resolving the infection process reveals
782 striking differences in the contribution of environment, genetics and phylogeny to host-
783 parasite interactions. *BMC Biol.* 9:11.

784 Ebert D. 2005. Ecology, epidemiology, and evolution of parasitism in daphnia. Bethesda, Md.:
785 National Library of Medicine (US), National Center for Biotechnology Information. Available
786 from:
787 http://www.ncbi.nlm.nih.gov/books/bv.fcgi?call=bv.View..ShowTOC&rid=daph.TOC&depth=
788 2

789 Ebert D, Fields PD. 2020. Host–parasite co-evolution and its genomic signature. *Nat. Rev. Genet.*
790 21:754–768.

791 Ebert D, Rainey P, Embley TM, Scholz D. 1996. Development, life cycle, ultrastructure and
792 phylogenetic position of Pasteuria ramosa Metchnikoff 1888: rediscovery of an obligate
793 endoparasite of Daphnia magna Straus. *Philos. Trans. R. Soc. Lond. B. Biol. Sci.* 351:1689–
794 1701.

795 Fredericksen M, Ameline C, Krebs M, Hüssy B, Fields PD, Andras JP, Ebert D. 2021. Infection
796 phenotypes of a coevolving parasite are highly diverse, structured, and specific. *Evolution*
797 75:2540–2554.

798 Henriques AO, Moran CP Jr. 2007. Structure, assembly, and function of the spore surface layers.
799 *Annu. Rev. Microbiol.* 61:555–588.

800 Jombart T. 2008. adegenet: a R package for the multivariate analysis of genetic markers.
801 *Bioinformatics* 24:1403–1405.

802 Jombart T, Devillard S, Balloux F. 2010. Discriminant analysis of principal components: a new method
803 for the analysis of genetically structured populations. *BMC Genet.* 11:94.

804 Karlström Å, Jacobsson K, Flock M, Flock J-I, Guss B. 2004. Identification of a novel collagen-like
805 protein, SclC, in Streptococcus equi using signal sequence phage display. *Vet. Microbiol.*
806 104:179–188.

807 Korte A, Farlow A. 2013. The advantages and limitations of trait analysis with GWAS: a review. *Plant*
808 *Methods* 9:29.

809 Lees JA, Ferwerda B, Kremer PHC, Wheeler NE, Serón MV, Croucher NJ, Gladstone RA, Bootsma HJ,
810 Rots NY, Wijmega-Monsuur AJ, et al. 2019. Joint sequencing of human and pathogen
811 genomes reveals the genetics of pneumococcal meningitis. *Nat. Commun.* 10:1–14.

812 Legendre P, Desdevises Y, Bazin E. 2002. A statistical test for host–parasite coevolution. *Syst. Biol.*
813 51:217–234.

814 Li H. 2013. Aligning sequence reads, clone sequences and assembly contigs with BWA-MEM.
815 *ArXiv13033997 Q-Bio*.

816 Li H, Handsaker B, Wysoker A, Fennell T, Ruan J, Homer N, Marth G, Abecasis G, Durbin R, 1000
817 Genome Project Data Processing Subgroup. 2009. The Sequence Alignment/Map format and
818 SAMtools. *Bioinformatics* 25:2078–2079.

819 Luijckx P, Duneau D, Andras JP, Ebert D. 2014. Cross-species infection trials reveal cryptic parasite
820 varieties and a putative polymorphism shared among host species. *Evol. Int. J. Org. Evol.*
821 68:577–586.

822 Luijckx P, Fienberg H, Duneau D, Ebert D. 2013. A matching-allele model explains host resistance to
823 parasites. *Curr. Biol.* 23:1085–1088.

824 Lukomski S, Bachert BA, Squeglia F, Berisio R. 2017. Collagen-like proteins of pathogenic
825 streptococci. *Mol. Microbiol.* 103:919–930.

826 Marees AT, de Kluiver H, Stringer S, Vorspan F, Curis E, Marie-Claire C, Derks EM. 2018. A tutorial on
827 conducting genome-wide association studies: Quality control and statistical analysis. *Int. J.*
828 *Methods Psychiatr. Res.* [Internet] 27. Available from:
829 https://www.ncbi.nlm.nih.gov/pmc/articles/PMC6001694/

830 Märkle H, John S, Cornille A, Fields PD, Tellier A. 2021. Novel genomic approaches to study
831 antagonistic coevolution between hosts and parasites. *Mol. Ecol.* 30:3660–3676.

832 McElroy K, Mouton L, Du Pasquier L, Qi W, Ebert D. 2011. Characterisation of a large family of
833 polymorphic collagen-like proteins in the endospore-forming bacterium Pasteuria ramosa.
834 *Res. Microbiol.* 162:701–714.

835 Metzger CMJA, Pepijn L, Gilberto B, Mahendra M, Ebert D. 2016. The Red Queen lives: Epistasis
836 between linked resistance loci. *Evolution* 70:480–487.

837 Morand S. 2015. (macro-) Evolutionary ecology of parasite diversity: From determinants of parasite
838 species richness to host diversification. *Int. J. Parasitol. Parasites Wildl.* 4:80–87.

839 Naret O, Chaturvedi N, Bartha I, Hammer C, Fellay J, The Swiss HIV Cohort Study (SHCS). 2018.
840 Correcting for population stratification reduces false positive and false negative results in
841 joint analyses of host and pathogen genomes. *Front. Genet.* 9.

842 Paterson GK, Nieminen L, Jefferies JMC, Mitchell TJ. 2008. PclA, a pneumococcal collagen-like
843 protein with selected strain distribution, contributes to adherence and invasion of host cells.
844 *FEMS Microbiol. Lett.* 285:170–176.

845 Poulin R. 2011. Evolutionary ecology of parasites. 2nd ed. Princeton University Press

846 Qiu Y, Zhai C, Chen L, Liu X, Yeo J. 2021. Current insights on the diverse structures and functions in
847 bacterial collagen-like proteins. *ACS Biomater. Sci. Eng.*

848 R Core Team. 2016. R: A language and environment for statistical computing. Available from:
849 https://www.R-project.org/

850 Schmid-Hempel P. 2021. Evolutionary parasitology: the integrated study of infections, immunology,
851 ecology, and genetics. 2nd ed. Oxford University Press

852 Strong PCR, Fulton KM, Aubry A, Foote S, Twine SM, Logan SM. 2014. Identification and
853 characterization of glycoproteins on the spore surface of Clostridium difficile. *J. Bacteriol.*
854 196:2627–2637.

855 Vandersmissen L, De Buck E, Saels V, Coil DA, Anné J. 2010. A Legionella pneumophila collagen-like
856 protein encoded by a gene with a variable number of tandem repeats is involved in the
857 adherence and invasion of host cells. *FEMS Microbiol. Lett.* 306:168–176.

858 Wang M, Roux F, Bartoli C, Huard-Chauveau C, Meyer C, Lee H, Roby D, McPeek MS, Bergelson J.
859 2018. Two-way mixed-effects methods for joint association analysis using both host and
860 pathogen genomes. *Proc. Natl. Acad. Sci.*:201710980.

861 Wickham H, Chang W, Henry L, Pedersen TL, Takahashi K, Wilke C, Woo K, RStudio. 2018. ggplot2:
862 Create Elegant Data Visualisations Using the Grammar of Graphics. Available from:
863 https://CRAN.R-project.org/package=ggplot2

864 Xu Y, Keene DR, Bujnicki JM, Höök M, Lukomski S. 2002. Streptococcal Scl1 and Scl2 proteins form
865 collagen-like triple helices *. *J. Biol. Chem.* 277:27312–27318.

866 Zhou X, Stephens M. 2012. Genome-wide efficient mixed-model analysis for association studies. *Nat.*
867 *Genet.* 44:821–824.

868

869 **FIGURES**

870 **Figure 1. G**enomic diversity and population structure of samples used in this study. **(A)** Per
871 sample levels of genomic diversity for *P. ramosa,* expressed as the proportion of population-
872 wide variant sites showing within sample polymorphism. Single genotype infections of the
873 haploid *P. ramosa* are expected to show values near zero, while larger values indicate
874 multiple infections. Values > 0.15 represent infections from multiple distinct pasteuria
875 lineages (shaded in red), with lesser values indicating multiple infections of closely related
876 genotypes (blue). **(B)** PCA ordination of parasite genomes (N = 248) recovered from infected
877 hosts. Parasites cluster into three primary genomic groups (*Alpha*, *Beta*, *Gamma*), with
878 membership derived by DAPC clustering of whole-genome data. The colors of the points
879 represent DAPC clusters. Open circles represent multiple infections containing mixtures of
880 genotypes from different clusters (red shaded area on panel A). **(C)** The same PCA ordination
881 rotated to show PCs 1 and 3. The *Alpha* cluster shows relatively continuous variation across
882 the PC 3, which DAPC clustering hierarchically sub-divides into *Alpha-1* and *Alpha-2* /
883 *Alpha-3.* Note the relatively modest contribution to total genomic variation by PC 3 relative
884 to the first two PCs. **(D)** Per sample levels of genomic diversity for *D. magna*, where each
885 sample represents a single diploid individual**. (E)** PCA ordination of *D. magna* samples (N =
886 248) plotted across the first two principal components. Note the low percentage of variance
887 explained by the primary axes and the lack of overall structure. DAPC clustering for *D.*
888 *magna* best supports a single cluster. **(F)** PCA scree plots for *P. ramosa* and *D. magna.*

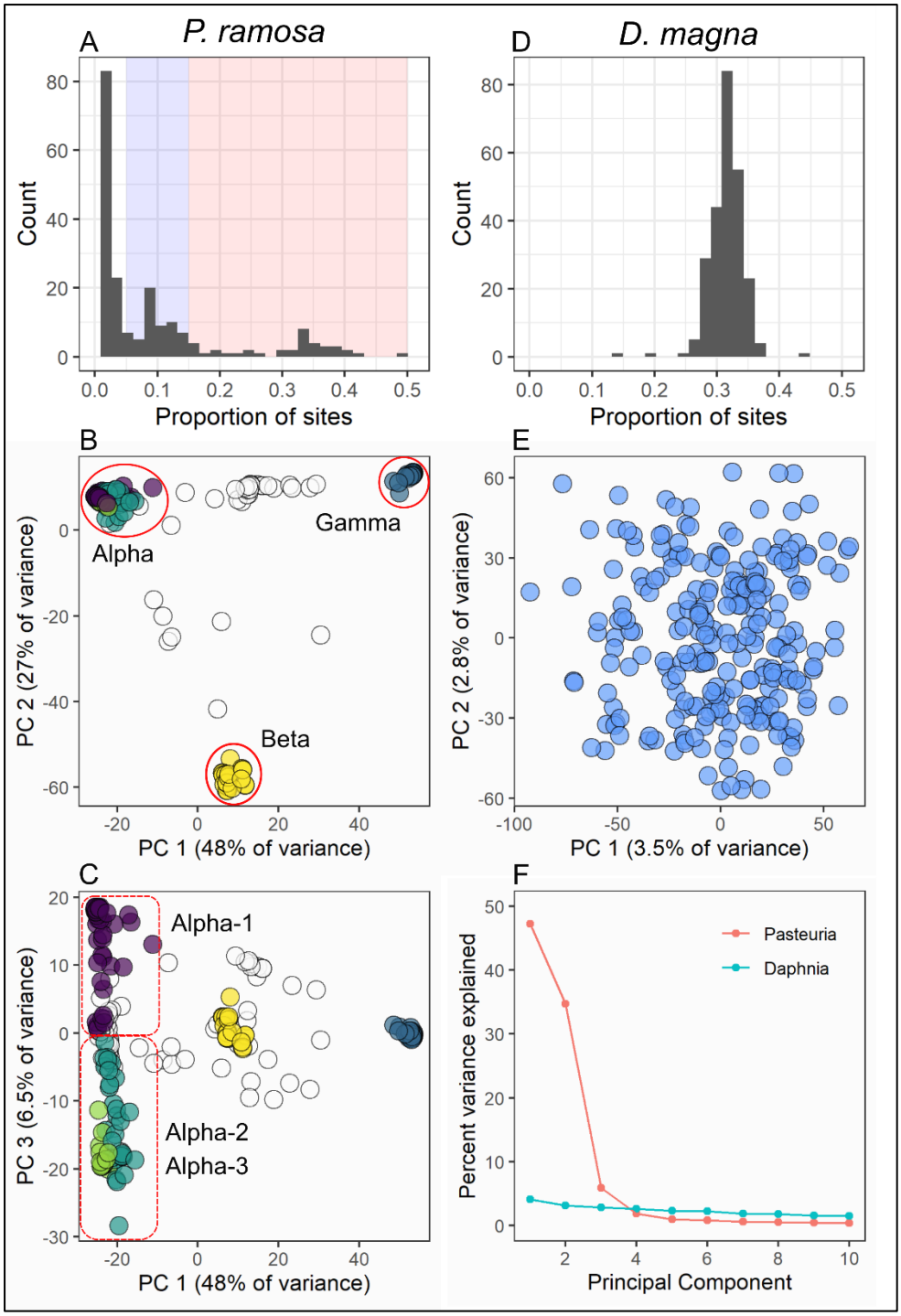
A
P. ramosa
Count
Proportion of sites
D
D. magna
Count
Proportion of sites
B
Alpha
Gamma
Beta
PC 2 (27% of variance)
PC 1 (48% of variance)
E
PC 2 (2.8% of variance)
PC 1 (3.5% of variance)
C
Alpha-1
Alpha-2
Alpha-3
PC 3 (6.5% of variance)
PC 1 (48% of variance)
F
Pasteuria
Daphnia
Percent variance explained
Principal Component

889

890 **Figure 2.** The 500 strongest associations for each co-GWAS model between variants in the
891 host genome (bottom ring segments) and the parasite genome (top segments). Inner ring
892 segments (gray background) indicate the scaled genomic position (x-axis) and strength (y-
893 axis) of the association, expressed as the p-value of the co-GWAS score on a -$\log_{10}$ scale.
894 Outer ring segments (with blue background) indicate nucleotide diversity (π), scaled from 0
895 to 1. Darker pathways indicate a greater number of associations, with known resistance loci
896 of the host being shown in blue, red, and green (C, D, and E locus, respectively). Outer red
897 bars indicate the position of PCL gene triplets in the *P. ramosa* genome and resistance genes
898 in the *D. magna* genome; the outer ring of the host genome displays chromosome numbers.
899 Model 1 shows a strong association between the host C locus and a dense cluster of PCL
900 gene triplets in the parasite genome. Model 2 shows the C locus (as in model 1), but also
901 shows a strong association between the host D locus and a different PCL gene triplet in the
902 parasite genome. In model 3 the strongest associations occur on two regions of chromosome
903 5: One region coincides with the previously described E locus for pasteuria resistance, the
904 other corresponds to a previously undescribed candidate locus for pasteuria resistance which
905 may interact with the E locus (see main text). Lines shown in purple pertain to a new
906 candidate locus for *Pasteuria* resistance.

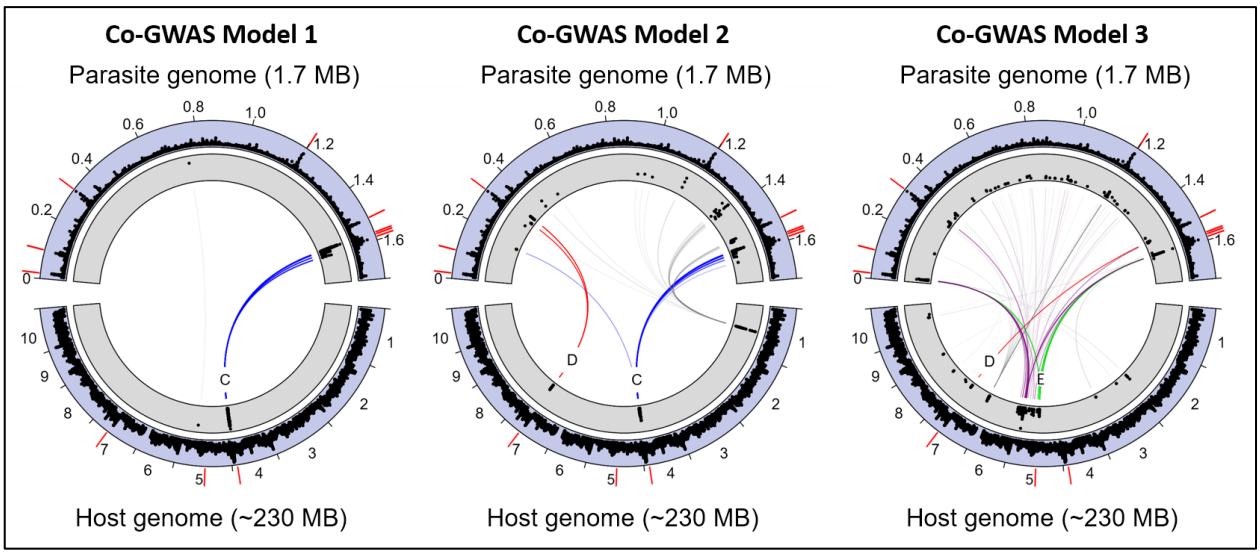

907 **Figure 3.** Single phenotype GWAS for resistance to the *P. ramosa* isolate P20. Resistance or
908 susceptibility to this isolate is diagnostic of the allelic state at the E locus. The positions of
909 the C locus (blue), D locus (red), E locus (green) and new candidate locus for *Pasteuria*
910 resistance (purple) are indicated by vertical bars. Our results show a strong peak at the
911 position of the E locus (green) as expected from previous studies. However, we observe a
912 much stronger peak on the right arm of chromosome 5 (purple) that coincides with the
913 primary peak from our third co-GWAS model. This result provides further evidence of a
914 uncharacterized pasteuria resistance locus at this position, which may epistatically interact
915 with the E locus.

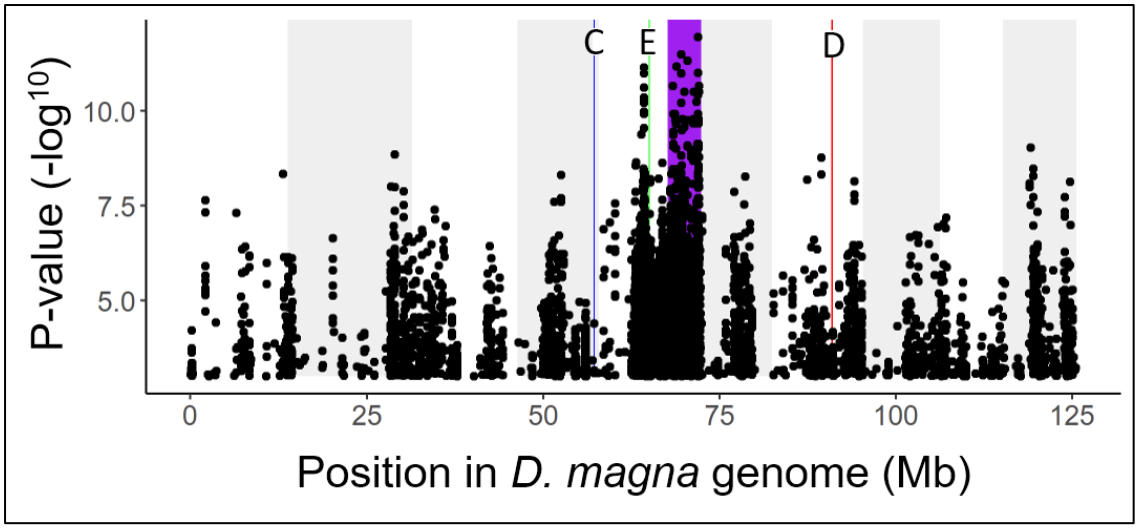

916

Figure 4. Contingency tables of genotype clusters at host resistance loci (derived via DAPC) versus *P. ramosa* genomic cluster. Cells are colored according to the magnitude and direction of deviation from the expected number of observations (Pearson residuals), with host and parasite combinations occurring more often than expected shown in red, and less often in blue. Host genotype clusters are characterized as resistant or susceptible relative to their diagnostic *P. ramosa* isolates – none are universally susceptible or resistant. Residuals for host-parasite combinations were calculated from a chi-squared contingency table test ($p < 0.001$ for all matrices, see text for full result) and then rescaled from -1 to 1 for color plotting. Numbers inside cells are the counts for each combination. Multiple infections (open circles on panel B) are not included here, resulting in a total count of 171 in each table.

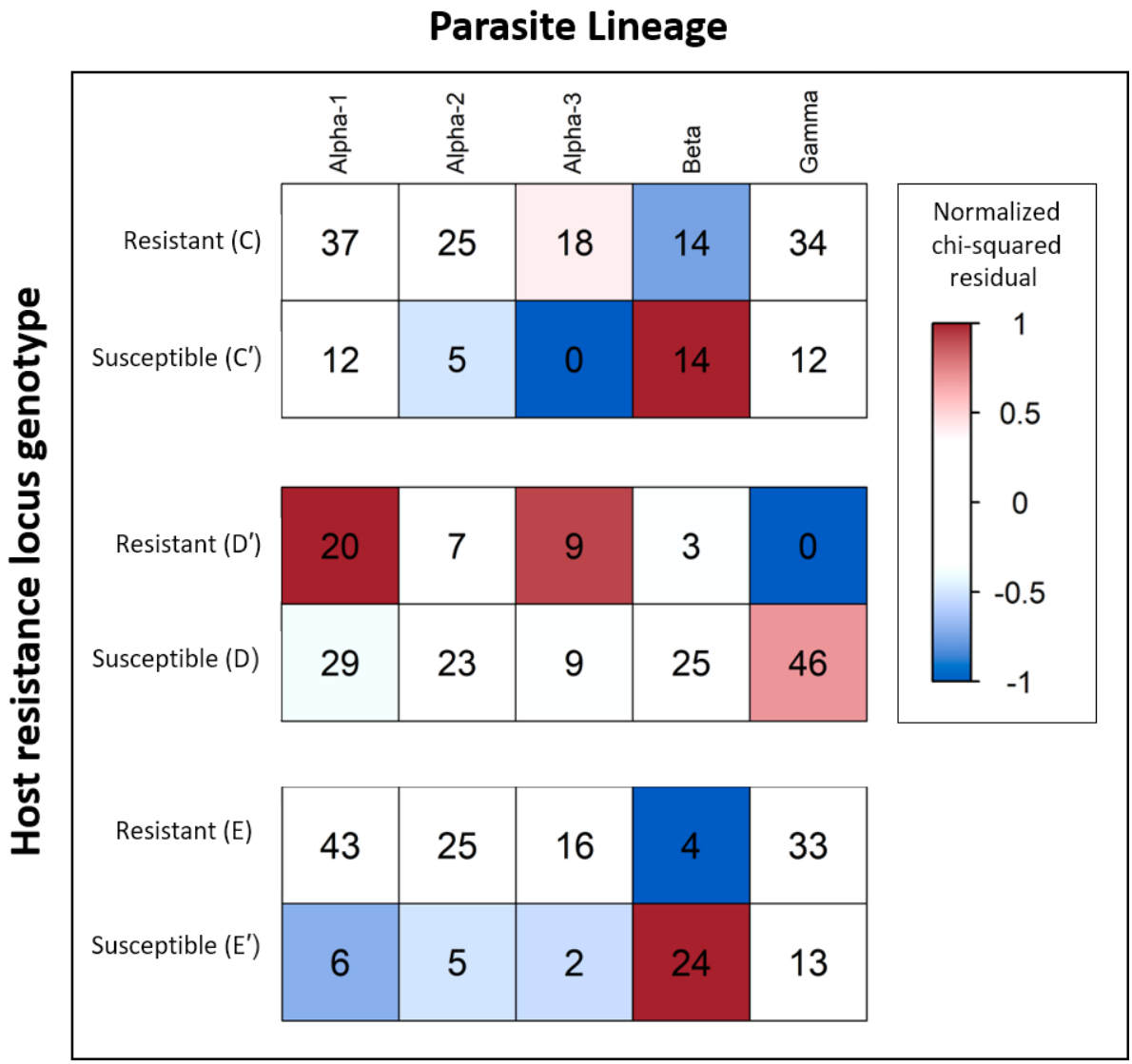

Table 1. Summary of top model results from each co-GWAS model. Rather than set a specific p-value threshold for statistical significance, the peaks described below represent the top 500 associations for each model as plotted in figure 2.

Model	Peak position (*D. magna*)	Peak description (*D. magna*)	Peak position (*P. ramosa*)	Peak description (*P. ramosa*)
1	Chromosome 4 (right arm) Contig 11: 2084705 – 2382802	Overlaps the C locus	1565875 – 1600196	Overlaps PCL triplets [9-10-11], [12-13-14], and]36-37-38]
	Chromosome 5 (right arm) Contig 71: 160694	Single SNP, intragenic, possible mapping error	758063	Aminofutalosine synthase (electron transport)
2	Chromosome 4 (right arm) Contig 11: 2084705 – 2357097	Overlaps the C locus	1565739 – 1628258	Overlaps PCL triplets [9-10-11], [12-13-14], and [36-37-38]
	Chromosome 7 (right arm) Contig 18: 1785587 – 1803392	Overlaps the D locus	318169 – 343599	Overlaps PCL triplet [21-27-28]
	Contig 32: 849103	Single SNP, intragenic, possible mapping error	1347536 – 1382775	IMP dehydrogenase and DNA topoisomerase subunit B
3	Chromosome 5 (left arm) Contig 1: 6277551 – 6506684 Contig 67: 230263 – 233072	Overlaps the E locus	1588560 – 1588747	Overlaps PCL triplet [36-37-38]
			4530 – 4707	3 Kb from PCL triplet [6-7-8]
	Chromosome 5 (right arm) Contig 25: 43625 – 1636178 Contig 53: 182869 – 443318	Shows strong correlation with resistance to *P. ramosa* isolates P20	4530 – 8506	Overlaps PCL triplet [6-7-8]
			319494 – 319584	Overlaps PCL triplet [21-27-28]
			1519089 – 1520569	Overlaps PCL triplet [24-25-26]
			1588269 – 1589748	Overlaps PCL triplet [36-37-38]
	Chromosome 7 (left arm) Contig 3: 4270730 – 4354576	Mostly uncharacterized genes	1181208 – 1205486	Overlaps PCL triplet [15-16-17]
	Chromosome 7 (right arm) Contig 18: 1785587 – 1802479	Overlaps the D locus	1516194	1 Kb distant from PCL triplet [24-25-26]